Soft Matter

Cite this: *Soft Matter*, 2012, **8**, 10017

www.rsc.org/softmatter

PAPER

Synthesis and self-assembly of nonamphiphilic hyperbranched polyoximes†

Yue Jin,[a] Liang Song,[a] Dali Wang,[a] Feng Qiu,[a] Deyue Yan,[a] Bangshang Zhu[b] and Xinyuan Zhu*[ab]

Received 16th May 2012, Accepted 19th June 2012
DOI: 10.1039/c2sm26124c

Nonamphiphilic hyperbranched polyoximes (HPOXs) were successfully synthesized by the polycondensation of trialdehyde and bis-aminooxy monomers with different molar feeding ratios. Various characterization techniques, such as 1D and 2D nuclear magnetic resonance (NMR), Fourier transform infrared spectroscopy (FTIR), and multi-detector gel permeation chromatography (GPC) were used to identify the highly branched structure of the HPOXs. Despite there being no amphiphilic block segments, HPOXs with a torispherical structure could self-assemble into nanoparticles in a mixed solution of dimethyl sulfoxide and H_2O. Besides, the modulation of the degree of branching (DB) and the terminal groups resulted in the appearance of spherical and bowl-shaped morphologies due to the change of the intra- and inter-molecular interactions. Accordingly, dynamic light scattering (DLS), transmission electron microscopy (TEM), atomic force microscopy (AFM), scanning electron microscopy (SEM), fluorescence spectroscopy (FL) together with ultraviolet and visible spectrometery (UV-vis) were employed to unravel the tentative mechanism of the formation of the HPOX self-assemblies. Moreover, dynamic oxime linkages and hydrogen bonds endowed the HPOX nanoparticles with pH and thermal dual responsiveness, which was confirmed by TEM measurements. HPOXs are developed to offer a novel pathway for the design of nonamphiphilic self-assemblies with dual responsiveness.

Introduction

The solvophilic–solvophobic interaction of amphiphilic polymeric blocks can fabricate common nanoparticles with typical core–shell structure or other morphologies. From the traditional perspective of self-assembly, the distinct amphiphilic structure is indispensable for the formation of polymeric nanoparticles. For nonamphiphilic polymers, it is difficult to provide enough inter- and intra-molecular interactions to drive the formation of nanoparticles. Therefore, the design of nonamphiphilic structures that can spontaneously aggregate into micelles has greatly challenged the common self-assembly principle of synthetic macromolecules.[1,2]

As a matter of fact, natural assemblies without a well-defined separation of the hydrophilic–hydrophobic blocks, such as protein folding, are ubiquitous. The subunits or peptide chains of sophisticated proteins intertwine into coils and further converge into globular micelles, and the self-assembled structures are closely related to their functions. It's clear that noncovalent interactions like multiple hydrogen bonding interactions play a crucial role in the physical structures and chemical functions of natural aggregates, the manipulation of which allows access to excellent bio-inspired materials with versatile building blocks.[3–11] Similar to natural proteins, nonamphiphilic dendritic polymers are blessed with intrinsic torispherical conformation and numerous functional groups, which provide sufficient sites for supramolecular interactions and self-assembly. Furthermore, the adjustment of branched architecture and functional terminals is capable of effectively altering the supramolecular interactions. Hence, it can be imagined that by means of mimicking the structures and interactions of natural biomacromolecules, the self-assembly of nonamphiphilic synthetic polymers might be realized.

In this work, a three-dimensional hyperbranched polyoxime (HPOX) incorporating dynamic oxime bonds, numerous amide groups and aminooxy terminals, was prepared by the polycondensation of bis-aminooxy and trialdehyde.[12–14] As expected, the novel HPOXs without defined amphiphilic segments could self-assemble into nanoparticles, attributed to the inter- and intra-molecular multiple noncovalent interactions.[15,16] In particular, changing the surface functional groups and branched

[a]*School of Chemistry and Chemical Engineering, State Key Laboratory of Metal Matrix Composites, Shanghai Jiao Tong University, 800 Dongchuan Road, Shanghai 200240, People's Republic of China*
[b]*Instrumental Analysis Center, Shanghai Jiao Tong University, 800 Dongchuan Road, Shanghai 200240, People's Republic of China. E-mail: xyzhu@sjtu.edu.cn; Fax: +86-21-34205722; Tel: +86-21-34205699*

† Electronic supplementary information (ESI) available: mass spectrum of TBA. The dendritic, linear and terminal structural units of the HPOXs are listed and the DB of the HPOXs was calculated by quantitative ^{13}C NMR spectroscopy. The TGA and DSC curves of the HPOXs with different molar feeding ratios of trialdehyde to bis-aminooxy monomers. An AFM image of HPOX 3. ^{1}H NMR spectra of HPOX 4 in a mixture of DMSO-d_6 and D_2O and the degradability of the oxime bonds after adding HCl for 4 h. See DOI: 10.1039/c2sm26124c

architecture of the HPOX led to the morphological transformation from spherical to bowl-shaped micelles.[17–19] Both oxime linkages and hydrogen bonds endowed the HPOXs with stimuli responsiveness. The self-assembly of nonamphiphilic dendritic polymers provides a new strategy for designing stimuli-responsive nanostructures with a vast potential for further applications.

Experimental section

Materials

O,*O*′-1,3-Propanediylbishydroxylamine (PBH, Aldrich, 99%), terephthalaldehydic acid (TPA, TCI, >98%), *N*-hydroxysuccinimide (NHS, Acros, >98%), 1,3-dicyclohexylcarbodiimide (DCC, Aldrich, 99%), tris(2-aminoethyl) amine (TAA, Alfa Aesar, 97%) and 1,6-diphenyl-1,3,5-hexatriene (DPH, 98%) were used as received without further purification. *N*,*N*-Dimethylformamide (DMF) and dimethyl sulfoxide (DMSO) were used after purification by distillation under vacuum and dried with calcium chloride ($CaCl_2$) and calcium hydride (CaH_2), respectively. Dichloromethane, chloroform and isopropanol were refluxed with CaH_2, and then distilled prior to use. All other reagents and solvents of analytical grade were purchased from Sinopharm Chemical Reagent Co., Ltd and used as received unless otherwise mentioned.

Characterization

Nuclear magnetic resonance (NMR) spectroscopy. ^{1}H and ^{13}C NMR analyses were recorded on a Varian Mercury Plus 400 MHz spectrometer with deuterated dimethyl sulfoxide (DMSO-d_6) and deuterated chloroform ($CDCl_3$) as solvents at 20 °C. Tetramethylsilane (TMS) was used as the internal reference. ^{13}C, ^{1}H-heteronuclear singular quantum correlation (HSQC) and ^{13}C, ^{1}H-heteronuclear multiple bond correlation (HMBC) were carried out using a Bruker Avance III 400 spectrometer with DMSO-d_6 as the solvent. Quantitative ^{13}C NMR spectra were measured by the method of inverse gated ^{1}H decoupling.

Mass spectroscopy (MS). The purity was analyzed by quatropde-time of flight mass spectrometer (Q-TOF-MS) measurements, which were performed on a Waters-ACQUITYTM UPLC & Q-TOF-MS Premier with acetonitrile as the solvent.

Fourier transform infrared (FTIR) spectroscopy. FTIR spectra were measured by the KBr sample holder method on a Perkin Elmer Paragon 1000 instrument in the range 3600–400 cm^{-1}.

Gel permeation chromatography (GPC). The molecular weights and the Mark–Houwink–Sakurada parameters were determined on a Viscotek GPCMax VE2001 instrument with a quadruple-detector (differential refractive index (RI), UV-vis, differential viscometer (intrinsic viscosity, IV) and right-angle light scattering (RALS)). The GPC instrument was equipped with three Jordi polydivinylbenzene columns (Jordi FLP, Burlingham, MA) with pore sizes of 100 000, 10 000, and 1000 Å, respectively. The column temperature was set to 40 °C. HPLC-grade DMF (n = 1.430) with LiBr at a concentration of 0.05 M was used as the mobile phase at a flow rate of 1.0 mL min^{-1}. The multi-detector calibration of the optical constant was carried out with a poly(methyl methacrylate) (PMMA) standard (M_n = 750 000 g mol^{-1}, PDI = 1.12). The molecular weight and the polydispersity index (PDI) were calculated using OmniSEC 3.1 software.

Differential scanning calorimetry (DSC). DSC was performed on a TA Q2000 series in a nitrogen atmosphere. Indium and zinc standards were used for temperature and enthalpy calibration. First, the samples were heated from room temperature to 200 °C, held at this temperature for 3 min to remove the thermal history and then slowly cooled to −50 °C at 10 °C min^{-1}. Subsequently, the samples were heated again from −50 °C to 200 °C at 10 °C min^{-1} to determine their glass transition temperatures (T_g).

Thermal gravimetric analysis (TGA). TGA measurements were performed on a Perkin-Elmer TGA-7 thermo-gravimetric analyzer to investigate the thermal stability of all the samples in a nitrogen atmosphere from 40 °C to 700 °C at 20 °C min^{-1}.

Dynamic light scattering (DLS). DLS measurements were performed with a Malvern Zetasizer Nano S instrument (Malvern Instruments Ltd) equipped with a 4.0 mW He–Ne laser operating at λ = 633 nm. All samples (1 mg mL^{-1}) were measured at a scattering angle of 173° in aqueous solution at room temperature (25 °C).

Transmission electron microscopy (TEM). TEM studies were performed with a JEOL JEM-100CX-II instrument at a voltage of 200 kV. Samples were prepared by drop-casting micelle solutions onto carbon-coated copper grids, and then air-drying at room temperature before measurement.

Atomic force microscopy (AFM). The morphology was visualized using an atomic force microscope (AFM) with a tapping mode and a Nanoscope IIIa controller (Bruker, Veeco/DI). Tip information: radius <10 nm, cantilever length 90 ± 5 μm; width 40 ± 3 μm; thickness 2.0 ± 0.5 μm, resonant frequency 330 kHz, force constant 48 N m^{-1}.

Scanning electron microscopy (SEM). The morphology was visualized using a scanning electron microscope after gold sputtering treatment (FEI Nova NanoSEM 230 LV UHR FE-SEM OxFORD INCA X-Max 80 SDD EDS).

Fluorescence spectroscopy (FL). The fluorescence spectra were measured on a QM/TM/IM steady-state and time-resolved fluorescence spectrofluorometer in the range 375–700 nm. (Excitation wavelength λ_{ex} = 360 nm).

Synthesis of *N*-succinimidyl 4-formylbenzoate[20]

TPA (3 g, 22.4 mmol) and NHS (2.3 g, 20 mmol) were dissolved in a mixture of DMF (10 mL) and dichloromethane (27 mL) under an argon atmosphere. The solution was cooled to around 0 °C in an ice–salt bath, followed by gradually adding 4 mL of a dichloromethane solution of DCC (4.1 g, 20.0 mmol) in an airtight reaction vessel. After removing the ice–salt bath, the vessel was continuously stirred at room temperature overnight.

The precipitated *N*,*N*′-dicyclohexylurea (DCU) was removed by filtration. Dichloromethane was removed from the filtrate by rotatory evaporation and the remaining solution was frozen in liquid nitrogen and lyophilized to remove the DMF solvent. The dry residue was dissolved in 135 mL of isopropanol under reflux. The hot solution was immediately filtered and then cooled to room temperature. Subsequently, the precipitate was collected by filtration and dried under vacuum at 45 °C for 24 h. A white product was obtained. Yield: 2.5 g, 50%.

^{1}H NMR (400 MHz, $CDCl_3$, 298 K, ppm) δ: 2.92 (4H, s, –OCH_2CH_2CO–), 8.02 (2H, d, $J = 7.04$), 8.30 (2H, d, $J = 7.04$), 10.13 (1H, s, –C*H*O). ^{13}C NMR (400 MHz, $CDCl_3$, 298 K, ppm) δ: 25.86, 129.90, 131.47, 140.63, 161.12, 169.14, 191.77.

Synthesis of tris(2-(4-formylbenzamide) ethyl) amine[21–24]

TAA (243.7 mg, 5/3 mmol) was completely dissolved in 25 mL DMSO. The reaction at room temperature was initiated by adding another 25 mL DMSO solution of *N*-succinimidyl 4-formylbenzoate (1.236 g, 5 mmol). After 2 h, the vessel was filled with 100 mL H_2O. After another 2 h, the reaction solution was extracted with 3 × 40 mL chloroform. The mixed organic phase was washed with 50 mL water and dried by anhydrous magnesium sulfate ($MgSO_4$). After precipitation, the solvent was removed by rotary evaporation. The pale yellow solid tris(2-(4-formylbenzamide) ethyl) amine (TBA, N(CH_2CH_2NHCO–C_6H_4–*p*–CHO)$_3$) was sonicated in 250 mL water, filtered and dried under vacuum at 45 °C for 48 h to afford a slightly off-white powder. Yield: 0.57 g, 64%.

^{1}H NMR (400 MHz, DMSO-d_6, 298 K, ppm) δ: 2.73 (2H, t, –NCH_2–), 3.39 (2H, m, –CH_2NH–), 7.85 (2H, d, $J = 8.61$), 7.91 (2H, d, $J = 8.61$), 8.54 (1H, t, –CH_2N*H*–), 10.01 (1H, s, C*H*O). ^{13}C NMR (400 MHz, DMSO-d_6, 298 K, ppm) δ: 37.7, 53.7, 128.0, 130.0, 140.3, 167.3, 191.0.

Ulta performance liquid chromatography (UPLC) & Q-TOF-MS of TBA (Fig. S1†): calculated for $[M + H]^+$: 543.22, found *m*/*z*: 543.2244 $[M + H]^+$.

Synthesis of HPOXs with different molar ratios of monomers

An oximization polymerization procedure (where the molar feeding ratios of bis-aminooxy to trialdehyde vary from 0.8 to 1.5 in Table 1 and Table S1 in the ESI†) is as follows: PBH (59.68 mg, 1/3 mmol) was dissolved in anhydrous DMSO (5 mL) in a flask, and a DMSO solution (10 mL) of TBA (180.86 mg, 1/3 mmol) was added dropwise (the molar ratio of the two monomers was set at 1.0). The flask was consecutively evacuated and refilled with N_2 three times and then submerged in a 37 °C oil bath for 48 h. The light yellow reaction solution was transferred into a dialysis bag (MWCO = 3.5 kDa), which was enclosed in 2 L deionized water and dialyzed with renewed water for 48 h. After dialysis, the dialysis solution was frozen and lyophilized to a constant weight by a freeze-dryer system (Martin Christ, α1-4, Germany) at −56 °C for 48 h. The HPOXs with different DBs were obtained.

^{1}H NMR (400 MHz, DMSO-d_6, 298 K, ppm) δ: 2.07 (2H, br, –CH_2CH_2ONC–), 2.70 (2H, br, –NCH_2–), 3.32 (2H, br, –CH_2NH–), 4.24 (2H, br, –CH_2ONC–), 7.32 and 7.56 (2H, br, Ar), 7.48 and 7.75 (2H, br, Ar), 7.86 (2H, br, Ar), 7.90 (2H, br, Ar), 8.14 (2H, br, Ar), 8.25 (1H, br, –C*H*=NO–), 8.38 (1H, br, –CON*H*–), 8.55 (2H, br, –ONH_2), 10.00 (1H, br, C*H*O). ^{13}C NMR (400 MHz, DMSO-d_6, 298 K, ppm) δ: 29.3, 38.2, 39.5–40.8, 53.6, 71.2, 127.2, 128.2, 128.5, 130.0, 135.0, 135.7, 138.3, 140.0, 148.8, 166.4, 193.4.

Table 1 GPC data and thermal properties

Entry	HPOX 1	HPOX 2	HPOX 3	HPOX 4
TBA : PBH[a]	1 : 0.8	1 : 1.0	1 : 1.2	1 : 1.5
M_w[b] (×10^3)	6.2	12.3	31.7	49.8
PDI[b] (M_w/M_n)	1.7	3.2	4.2	4.4
α[b]	0.278	0.282	0.289	0.306
d*n*/d*c*[b]	0.139	0.229	0.223	0.191
DB[c]	0.51	0.38	0.32	0.23
$T_{d\text{-}10\%}$[d] (°C)	339.9	336.8	333.6	329.1
$W_{residue}$[d] (%)	31.5	30.7	22.5	25.8
T_g[e] (°C)	81.4	87.1	91.5	103.2

[a] The molar ratio of TBA to PBH. [b] Molecular weights, polydispersity and Mark–Houwink α determined by multi-detector GPC. [c] Degree of branching determined by quantitative ^{13}C NMR spectroscopy. [d] The temperature at 10% weight loss and the residual weight percentage at 700 °C determined by TGA. [e] The glass transition temperature determined by DSC.

Preparation of the HPOX micellar solution

Firstly, ~4 mg of the synthetic HPOXs were completely dissolved in 3.2 mL DMSO. Next, 0.8 mL deionized water was added dropwise under continuous stirring at room temperature, making a final HPOX concentration of 1 mg mL^{-1}. The resulting micellar solution was prepared to observe the morphology of the HPOXs. The appearance of turbidity in the solution indicated the formation of the aggregates.

Critical aggregation concentrations of self-assembled HPOX aggregates

Here, DPH was used as the UV-vis probe to investigate the critical aggregation concentration (CAC) of the HPOX self-assemblies. Initially, the appropriate concentration of the HPOX solution was prepared and diluted to various pre-set concentrations (from 0.1 mg mL^{-1} to 5.0 × 10^{-5} mg mL^{-1}) by DMSO solvent mixed with 20% H_2O. Secondly, a 0.5 mmol L^{-1} methanol solution of DPH was added into the serial solutions, making the DPH concentration at a constant of 5.0 × 10^{-6} mol L^{-1}. The set wavelength absorbance of 313 nm of all the solutions was recorded on a Perkin Elmer Lambda 20 UV-vis spectrometer. The points and the fitting lines were obtained and the horizontal ordinates of the turning points gave the CAC values of the different HPOX samples.

Thermo- and pH-responsiveness of the HPOX nanoparticles

For thermo-responsiveness, the HPOX 3 micellar solution was heated to 80 °C and then cooled to room temperature. The alteration of the turbidity was observed. The reversible diameter changes were monitored by DLS techniques between 25 and 85 °C. The equilibrium time at different temperatures was kept above 30 min. For pH-responsiveness, aqueous dilutions of trifluoroacetic acid (TFA) and triethylamine (TEA) were added into the HPOX 3 micellar solution, respectively. Subsequently,

the pH values were modulated at 4 and 10, respectively. After stirring for 3 h, observation of the turbidity of the aggregate solutions was made and TEM micrographs were taken to investigate the morphology of the aggregates at different pH values. Besides, the reversible diameter changes were monitored by DLS techniques in the different pH environments (pH 4, 10 and 7). The equilibrium time at the different pH values was kept above 30 min.

Results and discussion

Synthesis and characterization of the HPOXs

The synthetic route of the nonamphiphilic hyperbranched polyoximes (HPOXs) is illustrated in Scheme 1. HPOXs were prepared through the $A_2 + B_3$ oxime coupling reaction of the bis-aminooxy and tri-aldehyde monomers. Benefiting from the highly branched configuration, HPOXs possess a considerable number of end groups. By altering the molar feeding ratios of the A_2 to B_3 monomers, the terminal groups of the HPOXs can be readily converted from aldehydes to aminooxy functional groups. Both aldehyde and aminooxy groups are favorable for the effective adjustment of intra- and inter-molecular interactions and further modification, such as chemoselective ligations as robust biomolecular hooks.[25–31] To confirm the existence of the highly branched structure of the HPOXs, ^{1}H NMR, ^{13}C NMR, ^{13}C, ^{1}H-HSQC, and ^{13}C, ^{1}H-HMBC NMR techniques

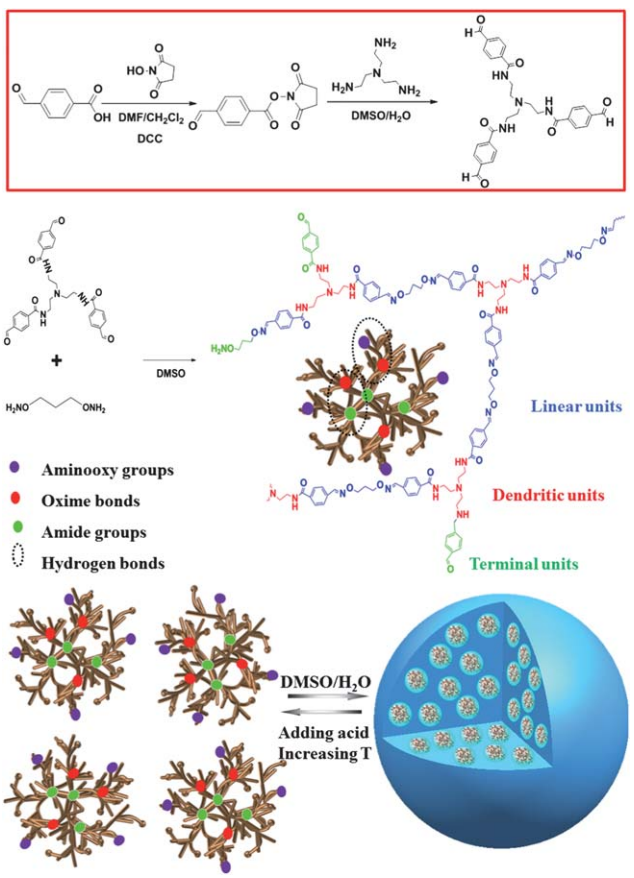

Scheme 1 Schematic representation of the synthetic route of the HPOXs and the tentative mechanism of the HPOX self-assembling behavior.

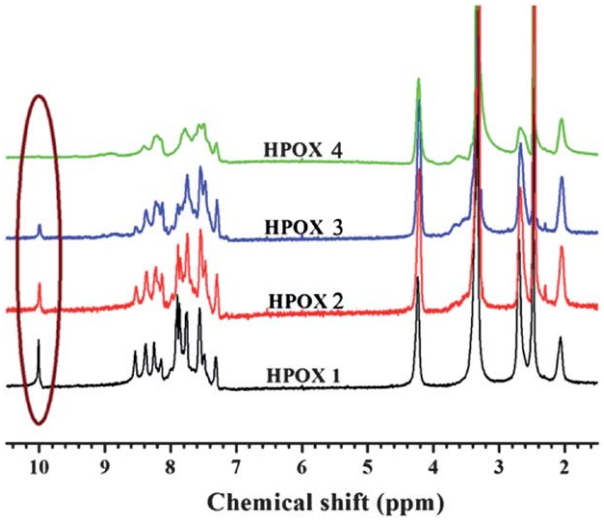

Fig. 1 ^{1}H NMR spectra of the HPOXs with different molar feeding ratios of trialdehyde to bis-aminooxy monomers.

were exploited. Fig. 1 shows the variation of the ^{1}H NMR spectra of the HPOX series. The proton signal at $\delta = 10.0$ ppm, assigned to the aldehyde end groups, is obviously impaired by increasing the amount of the bis-aminooxy monomer. The aldehyde signal disappears when the aminooxy/aldehyde ratio arrives at 1.5, confirming the complete reaction of the aldehyde terminals and thus the formation of the highly branched product.

The degree of branching (DB) is an important topological parameter for hyperbranched polymers. Generally speaking, the DB of hyperbranched polymers is determined by means of NMR analysis of the different structural fractions. The similar chemical environments among the dendritic units (D), the terminal units (T) and the linear units (L) in the dendritic structure of the HPOXs give rise to the overlapping signals in the ^{1}H NMR spectra between 7.2 and 8.6 ppm ascribed to the phenyl, oxime, amide and aminooxy protons, respectively. Accordingly, 2D ^{13}C,^{1}H-HMBC and ^{13}C,^{1}H-HSQC spectra are employed to distinguish the overlapping peaks, and the assignments are given in Fig. 2. To calculate the DB, the D, L and T units of the HPOXs are listed in Fig. S2 in the ESI.† Correspondingly, the DB of the samples was determined according to the following equation:[32]

$$DB = (D + T)/(D + T + L)$$

For the HPOXs, the DB was calculated from quantitative ^{13}C NMR analysis. As shown in Table 1, the DB of the HPOX samples range from 0.23 to 0.51, substantiating the highly branched architecture.

The FTIR spectra in Fig. 3 indicate that the absorption band at 1707 cm^{-1} from the C=O stretching of the aldehyde terminals decreases with the increasing amount of bis-aminooxy and finally disappears. Simultaneously, the N–H absorption band at around 3420 cm^{-1} due to the asymmetrical stretching vibration of the aminooxy group is gradually separated from the broad O–H absorption band and becomes evident. The FTIR spectra demonstrate the successful control of the terminal groups with altering the monomer feeding ratios. Moreover, the FTIR

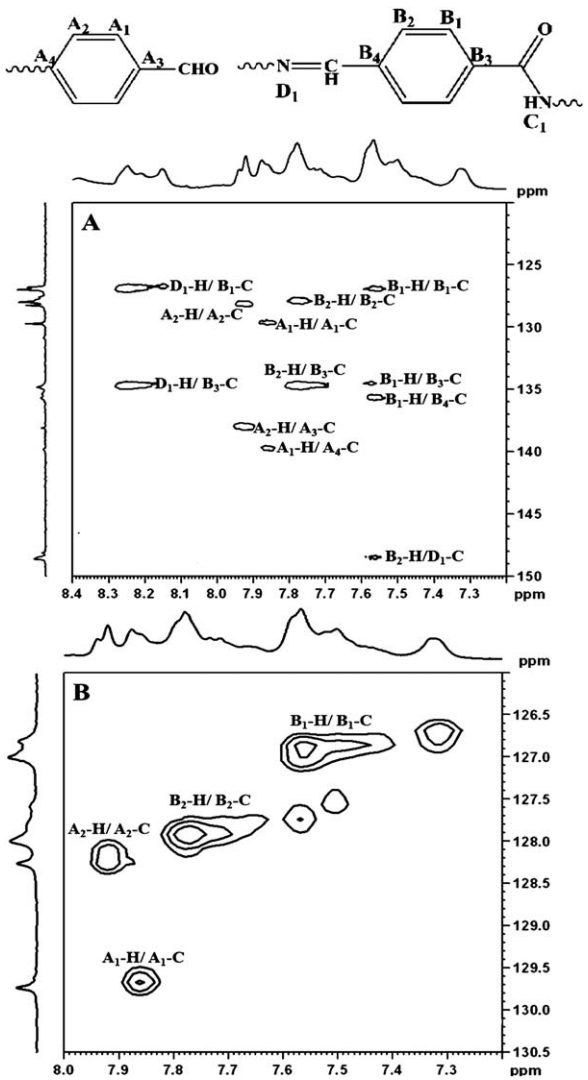

Fig. 2 The 2D NMR spectra of HPOX 3: (A) the ^{13}C,^{1}H-HMBC spectrum, and (B) the ^{13}C,^{1}H-HSQC spectrum.

spectra reveal the additional chemical structure information of the HPOX samples, which are consistent with the ^{1}H NMR analysis.

Molecular weight, thermal stability and solubility

The number-average molecular weight (M_n), polydispersity (M_w/M_n), viscosity-average molecular weight (M_η) and Mark–Houwink parameter (α) were measured by the multi-detector GPC technique. It should be mentioned that the molecular weight determination of hyperbranched polymers is still a problem to be solved. Given that the hydrodynamic volume of a hyperbranched polymer is smaller than that of the corresponding linear polymer with a similar molecular weight, the actual molecular weights of the HPOXs are supposed to be larger than the results from the multi-detector GPC test. As shown in Table 1, the molecular weights of the HPOXs increase with the amount of bis-aminooxy monomer, because the largest molecular weight can be obtained when the molar feeding ratio between the reactive aminooxy and aldehyde groups arrives at 1 during the

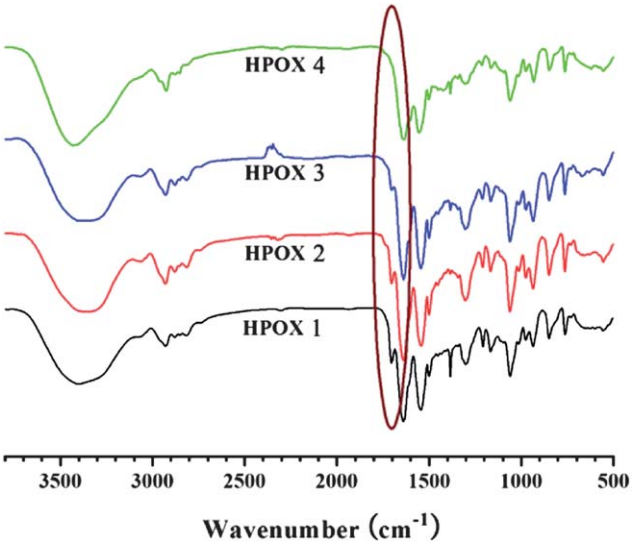

Fig. 3 The FTIR spectra of the HPOXs with different molar feeding ratios of trialdehyde to bis-aminooxy monomers.

polymerization. In contrast, the molecular weight declines when the ratios deviate from 1. Herein, the ratio of HPOX 4 is 1, so it is reasonable that its molecular weight is the largest. The Mark–Houwink parameter α is frequently used to reflect the branched structure of polymers based on the Mark–Houwink equation ($[\eta] = K \times M_\eta^\alpha$). From the Mark–Houwink fitting lines of the HPOX series, the parameter α lies between 0.27 and 0.31, confirming the formation of the hyperbranched structure. Additionally, the DSC and TGA curves are listed in Fig. S3 and S4 of the ESI.† The thermal stability of the HPOXs was investigated by TGA, wherein the $W_{residue}$ data reveals the high thermal stability of HPOX with above 25% of the residue remaining even at the high temperature of 700 °C. Based on the chemical structure of the HPOXs, it can be found that they belong to a kind of polyamide. Therefore, the HPOXs have a good thermal stability, especially due to the existence of the aromatic groups. After thermal degradation, the residues were observed to be black with very poor solubility in common organic solvents. According to the literature,[33–35] the residues may include organic carbide and certain aromatic derivatives under the inert atmosphere. The detailed GPC data together with the thermal properties of the HPOXs are summarized in Table 1. The solubility of the HPOXs was also investigated and all the HPOX samples manifested excellent solubility in common organic solvents, such as ethanol, DMSO and DMF. In terms of the traditional concept, the nonamphiphilic HPOXs weren't supposed to aggregate. Surprisingly, it was found that the synthetic HPOXs self-assembled into nanoparticles in a mixture of DMSO and H_2O. Therefore, a series of experiments were carried out to elucidate this phenomenon, and the tentative mechanism for the self-assembling behavior of the HPOXs in the mixed solution was proposed.

Investigation of HPOX self-assembly

To confirm the formation of the HPOX self-assemblies, UV-vis spectroscopy in conjugation with DLS, TEM, AFM, SEM and

fluorescence spectrometry was comprehensively exploited to prove the formation of the HPOX nanoparticles, illustrating the tentative mechanism for the self-assembling behavior of the HPOXs.

The CAC values of all the samples (HPOX 1, 2, 3, and 4) were measured by the UV-vis technique utilizing DPH as a probe. As shown in Fig. 4, the absorbance of DPH is near to zero while the concentration is below the CAC value, whereas the absorbance intensity of DPH is enhanced exponentially with concentration when the solvophobic DPH probe is packed in the micelles. Subsequently, the two fitting lines reflecting two states intersect at the turning point, the horizontal ordinate of which determines the CAC value. The CAC values of the HPOX samples are approximately close to each other in the same order of magnitude, approximately 10^{-2} mg mL^{-1}, exhibiting the opposite effect of the DB and hydrophilic–hydrophobic ratios of the HPOXs in the same mixed solution. The CAC determination verifies the formation of the HPOX micelles in the mixed media.

The hydrodynamic diameter and size distribution of the HPOX nanoparticles at the concentration of 1.0 mg mL^{-1} in the mixed DMSO–H_2O solvent were determined by the DLS technique, and the results are given in Fig. 5. With increasing amounts of the bis-aminooxy monomer, the average hydrodynamic diameters of the HPOX micelles increase from 282 nm to 582 nm. The polydispersity indexes (PDIs) of HPOX 1, 2, 3 and 4 are low, suggesting a narrow size distribution of these nanoparticles.

The morphologies of the as-prepared HPOX self-assemblies were observed by TEM, and the images are shown in Fig. 6. Consistent with the results of DLS, the TEM images indicate the increasing size of the HPOX 1, 2, and 3 nanoparticles with the increasing amount of the bis-aminooxy monomer. The sizes are smaller than those measured with the DLS technique, as TEM and DLS show different morphologies in the solid and swollen states, respectively. As illustrated in Fig. 6, the shapes of HPOX 1, 2 and 3 are different from that of HPOX 4. Correspondingly, the AFM and SEM images of HPOX 3 and HPOX 4 were measured to verify the formation of the HPOX nanoparticles with different morphologies. Both spherical and bowl-shaped

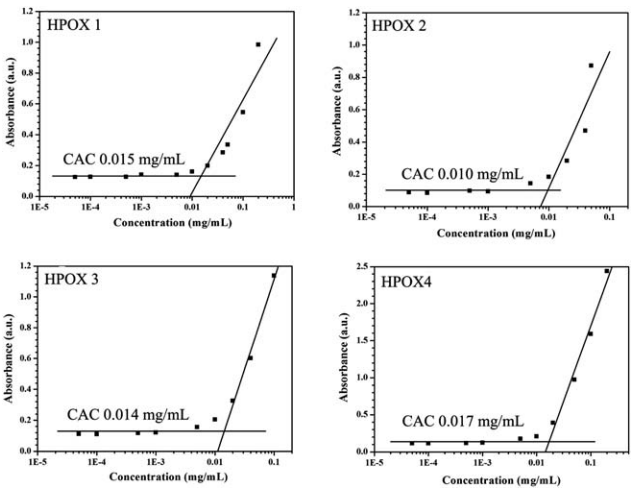

Fig. 4 The relationship of the absorbance intensity of DPH as a function of the concentration with the different HPOX samples.

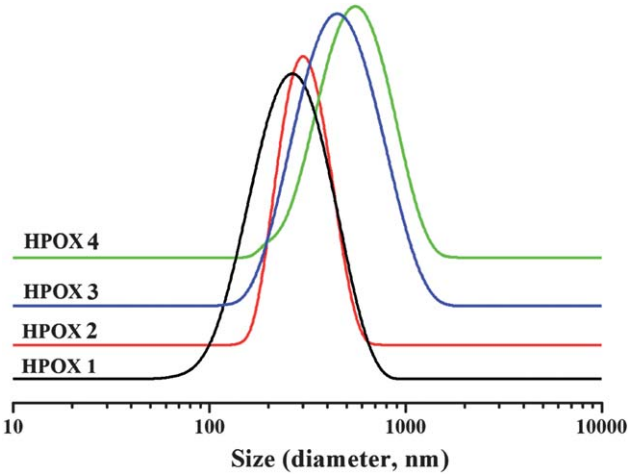

Fig. 5 DLS curves of the hydrodynamic diameters of the different HPOXs at a concentration of 1.0 mg mL^{-1}.

nanoparticles are observed in Fig. 7(b) and (d), and S5 of the ESI,† confirming the capability of controlling the morphologies of the nonamphiphilic micelles by changing the important structural parameters of the highly branched polyoximes. All the morphological data are listed in Table 2.

According to the previous report,[18,19] it was suggested that the formation of the bowl-shaped structure was kinetically controlled. At the beginning of the water addition to the HPOX–DMSO solution, the initial structure of the self-assembly is an apparently large sphere benefiting from the strong intermolecular interaction of the HPOX 4 chains, the viscosity of which is low. Therefore, the solvent molecules diffuse rapidly with the high chain mobility. Upon further addition of water, DMSO continues to be extracted through the surface of the sphere,

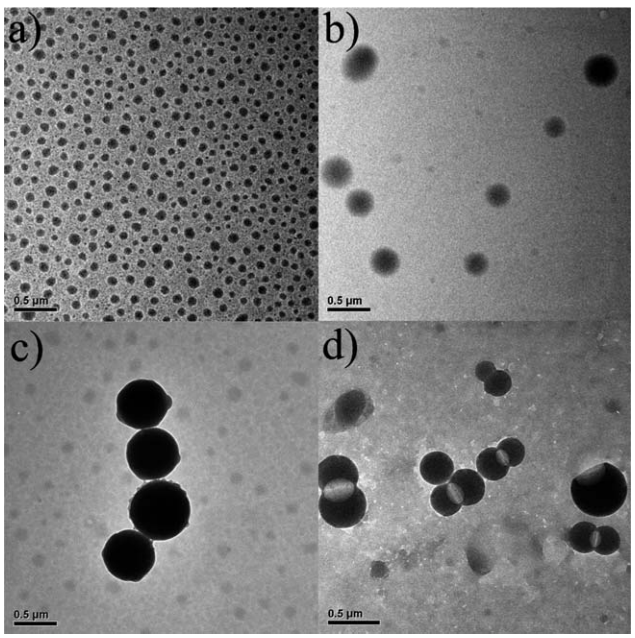

Fig. 6 TEM images of (a) HPOX 1, (b) HPOX 2, (c) HPOX 3, and (d) HPOX 4. (Scale bar: 500 nm).

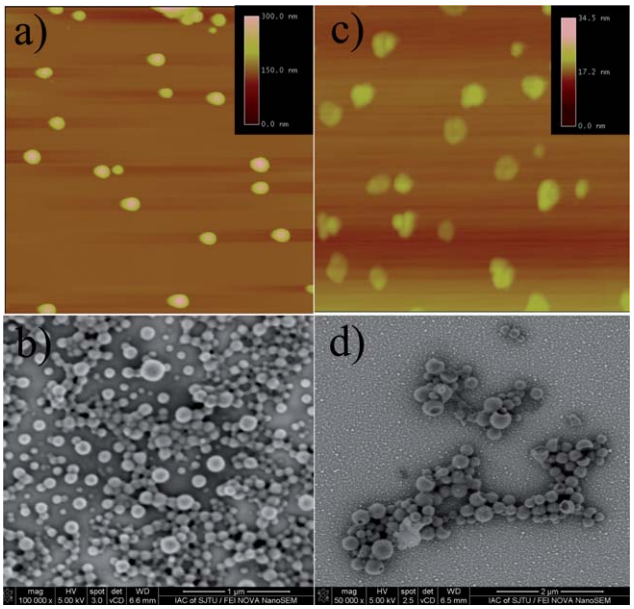

Fig. 7 HPOX 3 spherical self-assemblies: (a) AFM image (10 μm), (b) SEM image, and HPOX 4 bowl-shaped self-assemblies: (c) AFM image (10 μm), (d) SEM image.

Table 2 Morphological properties of HPOX aggregates (1.0 mg mL^{-1})

Entry	Diameter[a] (nm)	PDI[a]	TEM[b] (nm)	CAC[c] (mg mL^{-1})
HPOX 1	282	0.166	~150	0.015
HPOX 2	301	0.033	~250	0.010
HPOX 3	498	0.174	~480	0.014
HPOX 4	582	0.235	~550	0.017

[a] The average diameters and PDI determined by DLS. [b] The average diameters determined by TEM. [c] The CAC values determined by the UV-vis absorbance intensity of DPH.

leading to the high viscosity of the core. The low mobility of the HPOX chains can result in the external shell hardening. Alternatively, a liquid–liquid phase separation may occur. Subsequently, bubbles filled with the solvent-rich phase can form. The DMSO–water-filled bubbles are able to coalesce into a single bubble due to the good solubility and low viscosity of the highly branched architecture of HPOX 4, the driving force for which is the interfacial energy. The single bubble breaks through the surface but can't establish a spherical shape. Correspondingly, a bowl-shaped nanostructure can be formed. However, HPOX 1, 2, 3 don't form bowl-shaped nanoparticles, because the added viscosity-control mechanism plays an important role as well.[36] At the same water content, the added viscosity control of HPOX 4 is probably provided by more hydrogen bond interactions among the aminooxy groups at the periphery and the amide groups along the backbone in comparison with the samples of HPOX 3, 2 and 1 with decreasing amounts of aminooxy end groups. Therefore, the adjustment of the branched architecture can control the morphology of HPOX self-assemblies.

DMSO is the preferential solvent for HPOX, but H_2O provides poor solvation. In Fig. S6 of the ESI,† the ^1H NMR spectra of HPOX 4 in the mixture of DMSO-d_6 and D_2O with different D_2O volumes at 300 K were measured to demonstrate the effect of the water content on the self-assembling behavior of the nonamphiphilic nanoparticles in the mixed medium. Accordingly, the peak of oxime bonds disappears with the addition of water, indicating the inclination of the oxime bonds inside the nanoparticles due to the hydrophobicity. The introduction of H_2O transforms the conformation of the HPOXs in the mixed solution. It could be inferred that the intra- and intermolecular noncovalent interactions mainly stem from oxime bonds, aminooxy, amide and phenyl groups, hydrogen bonding interactions, π–π stacking interactions and the exchange of R groups of the oxime bonds (C═N–OR) with the aminooxy terminals, which may exert a great influence on the interwoven self-assembling structures.[37–39]

To explore the tentative mechanism, fluorescence emission spectroscopy was utilized to testify whether the π–π stacking interaction contributed to the self-assembling behavior. Fig. 8 shows that the fluorescence emission spectra of the HPOX 2 aggregates in the mixture apparently distinguish from that of the spectrum of HPOX 2 in pure DMSO, exhibiting an intense maximum at about 465 nm and a shoulder at 538 nm under an excitation wavelength of 360 nm. By comparison with the fluorescence spectrum before self-assembly, the micellar solutions of HPOX 2 with different volume ratios of DMSO to H_2O reveal the relatively higher emission intensity, demonstrating that the π–π stacking of phenyl rings doesn't emerge, otherwise it would result in luminescence quenching, which can greatly diminish the fluorescence emission intensity.[40] Hence, it can be inferred that the π–π stacking interaction may have little relationship with the interactions for aggregation. In other words, multiple hydrogen bonding interactions among the amide, oxime and aminooxy groups play the central role in HPOX micellization, which may cause the steric hindrance of the π–π stacking of the aromatic groups. As a result, the fluorescence emission doesn't diminish after self-assembly, as shown in Fig. 8. By adjusting the molecular conformation, the nonamphiphilic HPOXs with a torispherical structure can self-assemble into nanoparticles with spherical and bowl-shaped morphologies. The conformation

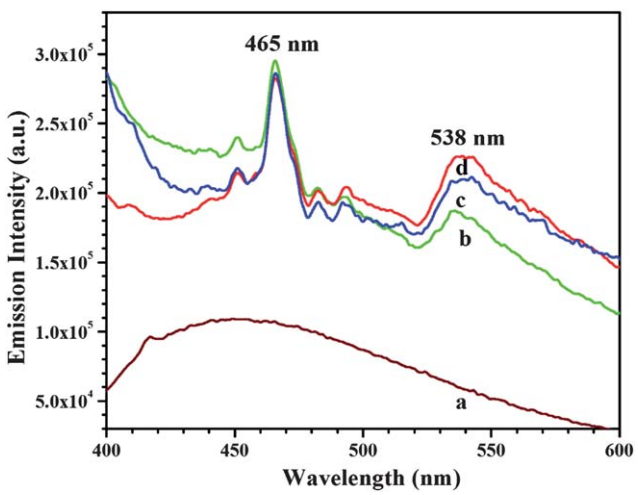

Fig. 8 Fluorescence emission spectra of (a) HPOX 2 in pure DMSO solvent, and HPOX 2 nanoparticles in DMSO–H_2O with different volume ratios of (b) 4 : 1, (c) 2 : 3, and (d) 1 : 4 (λ_{ex} = 360 nm).

alteration is driven by the intra- and inter-molecular interactions from the changes in the structural parameters of the HPOXs, which may mimic the route of the natural assemblies.

Thermal and pH dual responsiveness of HPOX self-assembly

The photographs in Fig. 9 present the apparent transformation of turbidity in a heating–cooling cycle for the observation of HPOX self-assemblies. When the micellar solution is gradually heated to 85 °C, the turbid mixed solution evidently becomes optically clear, indicating the dissociation of the HPOX aggregates with increasing temperature. Conversely, when cooled back to room temperature, it spontaneously returns to the former turbidity, suggesting the re-assembly of HPOX after disassembly. The reversible thermal-responsive property of the HPOX self-assemblies was further confirmed by the DLS technique. The diameter ratio between 25 and 85 °C is denoted by the formula of size/498. The result is in harmony with the proposed mechanism, which derives from hydrogen bonds and reversible oxime bonds. The high temperature accelerates the breaking of the weak linkages of the hydrogen bonds and oxime bonds.

The photos in Fig. 10 also exhibit the obvious discrepancy in turbidity of HPOX micellar solutions with varying pH values (4, 7 and 10), reflecting pH responsiveness. It should be mentioned that the hydrolysis of labile oxime bonds is catalyzed by general acids and bases. Both the dynamic oxime bonds and hydrogen bonds of the HPOXs are subjected more to the acidic conditions (pH 4) than the alkaline medium (pH 10).[41–43] At pH 4, the acidic conditions not only facilitate the destruction of the hydrogen

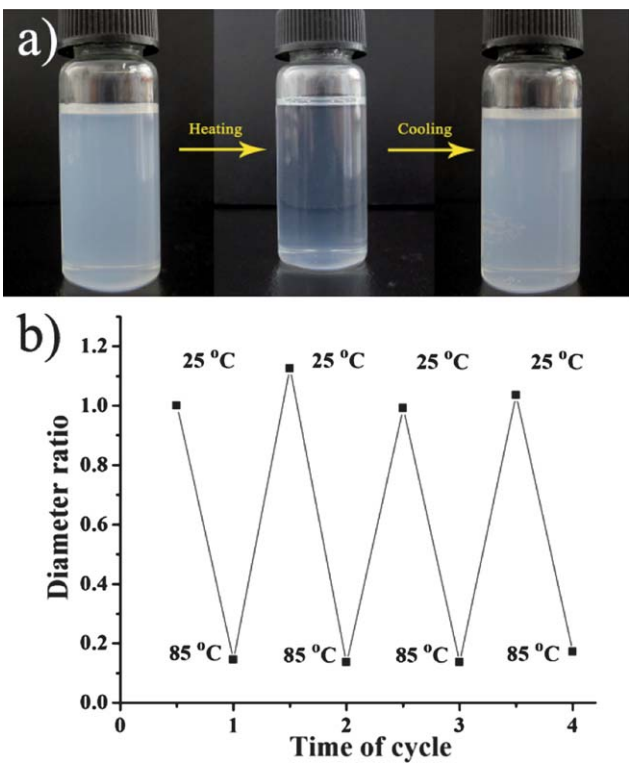

Fig. 9 (a) Photographs of the HPOX 3 self-assemblies with changing temperature, and (b) their reversible diameter changes at pH 7 between 25 and 85 °C. (Diameter ratio: size/498).

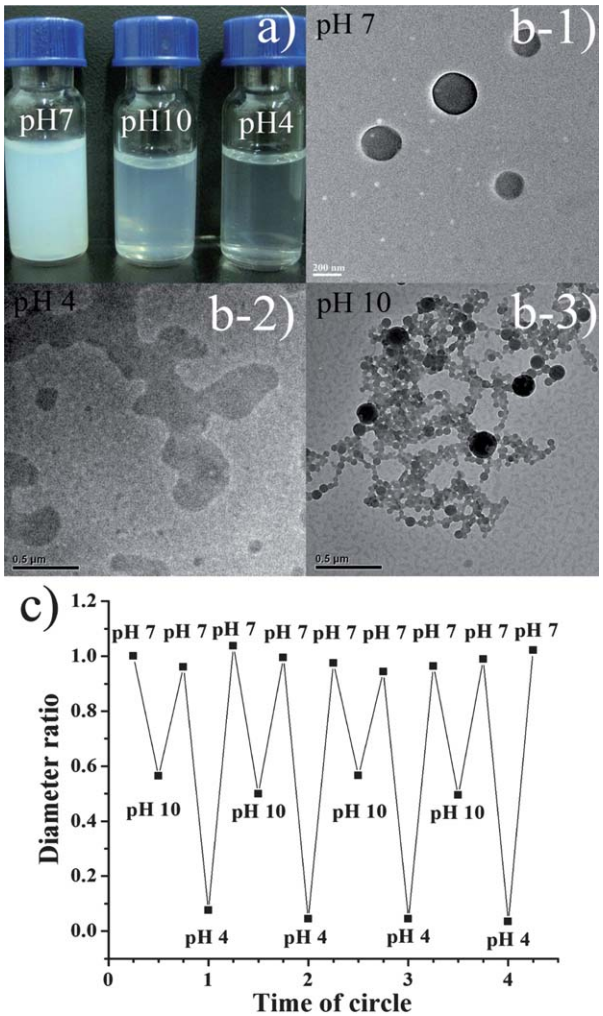

Fig. 10 (a) Photographs with altering pH, (b-1, b-2 and b-3) TEM images of the HPOX 3 self-assemblies (scale bars: 200 nm and 500 nm) with altering pH, and (c) their reversible diameter changes at 25 °C with altering pH (4, 10 and 7). (Diameter ratio: size/498).

bonding interactions by protonation, but also accelerate the hydrolysis of the conjugated oxime bonds. The breaking of both the hydrogen bonds and oxime bonds results in the complete disappearance of the turbidity of the HPOX micelles. The environment at pH 10 only catalyzes the reversible decomposition of part of the oxime bonds. Consequently, the breaking of these oxime bonds leads to the shrinking of the HPOX micelles into smaller ones, thus making the turbidity decrease. The TEM images in Fig. 10 provide potent support for the morphological changes with the different pH values (4, 7 and 10). As observed, the disruption of the HPOX micelles in the TEM micrographs occurs at pH 4, while the size of the nanoparticles diminishes at pH 10, the results of which are consistent with the alteration of the turbidity in the photo. Likewise, the reversible pH-responsive property of the HPOX self-assemblies was further confirmed by the DLS technique. The diameter ratio with altering pH values is denoted by the formula of size/498. The reversibility was monitored and confirmed by DLS for 4 cycles. Therefore, both the dynamic oxime covalent linkages and the transient noncovalent

hydrogen bonding interactions endow the HPOX aggregates with pH- and thermal-responsiveness.

As a result, the tentative mechanism for the formation of the HPOX nanoparticles and the reversible dual stimuli-responsiveness can be attributed to the noncovalent interactions of hydrogen bonds and oxime bonds.

Conclusions

Nonamphiphilic HPOXs were successfully prepared by the oxime coupling reaction of synthetic trialdehyde and bis-aminooxy, and the functional terminals of the HPOXs could be modulated by changing the molar feeding ratios of the A_2 and B_3 monomers. ^{1}H NMR, quantitative ^{13}C NMR, HSQC, HMBC and FTIR were exploited for analyzing the highly branched structures. UV-Vis analysis, in conjugation with DLS, TEM, AFM, SEM and FL confirmed the formation of the HPOX self-assemblies in the mixed DMSO–H_2O solution, with uniform topology. Through adjusting the structural parameters of the nonamphiphilic HPOXs, the morphologies of the nanoparticles varied from sphere to bowl shape due to the alteration in the intra- and inter-molecular noncovalent interactions. Furthermore, the pH and thermal dual responsiveness of the HPOX self-assemblies were investigated. The intra- and inter-molecular driving forces of the HPOX nanoparticles originated from the noncovalent interactions among the oxime bonds, aminooxy terminals and amide bonds, rather than the π–π stacking interactions of phenyl groups in the backbone. Primarily, the supramolecular interactions between the dynamic oxime bonds and the alkyl aminooxy groups play a crucial role in the formation of the HPOX micelles. Moreover, the nonamphiphilic HPOXs contain a vast number of amide groups, which afford more sites for multiple hydrogen bonding interactions as well. HPOXs are orchestrated to construct the novel nonamphiphilic micelles with stimuli responsiveness. Furthermore, the HPOX self-assemblies will render us with a profound understanding of the sophisticated self-assembling behavior of nonamphiphilic biomolecules. This ongoing work aims to further elucidate the detailed mechanism of the novel polymeric self-assemblies.

Acknowledgements

This work is sponsored by the National Natural Science Foundation of China (20974062, 30700175) and the National Basic Research Program 2009CB930400, the Shuguang Program (08SG14), the Shanghai Leading Academic Discipline Project (Project number: B202), and the China National Funds for Distinguished Young Scientists (21025417).

Notes and references

1 L. Wu, J. Lal, K. A. Simon, E. A. Burton and Y.-Y. Luk, *J. Am. Chem. Soc.*, 2009, **131**, 7430–7443.
2 E. Yoshida and S. Kunugi, *Macromolecules*, 2002, **35**, 6665–6669.
3 A. Fegan, B. White, J. C. T. Carlson and C. R. Wagner, *Chem. Rev.*, 2010, **110**, 3315–3336.
4 E. N. Salgado, R. J. Radford and F. A. Tezcan, *Acc. Chem. Res.*, 2010, **43**, 661–672.
5 B. Kokona, A. M. Kim, R. C. Roden, J. P. Daniels, B. J. Pepe-Mooney, B. C. Kovaric, J. C. de Paula, K. A. Johnson and R. Fairman, *Biomacromolecules*, 2009, **10**, 1454–1459.
6 T. J. Measey, R. Schweitzer-Stenner, V. Sa and K. Kornev, *Macromolecules*, 2010, **43**, 7800–7806.
7 G. Askarieh, M. Hedhammar, K. Nordling, A. Saenz, C. Casals, A. Rising, J. Johansson and S. D. Knight, *Nature*, 2010, **465**, 236–238.
8 J. Mondal, X. Zhu, Q. Cui and A. Yethiraj, *J. Phys. Chem. C*, 2010, **114**, 13551–13556.
9 N. l. Carulla, M. Zhou, E. Giralt, C. V. Robinson and C. M. Dobson, *Acc. Chem. Res.*, 2010, **43**, 1072–1079.
10 Y. Levy and J. N. Onuchic, *Acc. Chem. Res.*, 2005, **39**, 135–142.
11 E. N. Salgado, R. A. Lewis, J. Faraone-Mennella and F. A. Tezcan, *J. Am. Chem. Soc.*, 2008, **130**, 6082–6084.
12 Y. Ruff and J.-M. Lehn, *Biopolymers*, 2008, **89**, 486–496.
13 J.-M. Lehn, *Chem. Soc. Rev.*, 2007, **36**, 151–160.
14 S. J. Rowan, S. J. Cantrill, G. R. L. Cousins, J. K. M. Sanders and J. F. Stoddart, *Angew. Chem., Int. Ed.*, 2002, **41**, 898–952.
15 V. A. Polyakov, M. I. Nelen, N. Nazarpack-Kandlousy, A. D. Ryabov and A. V. Eliseev, *J. Phys. Org. Chem.*, 1999, **12**, 357–363.
16 J. Liu, W. Huang, Y. Pang, P. Huang, X. Zhu, Y. Zhou and D. Yan, *Angew. Chem., Int. Ed.*, 2011, **50**, 9162–9166.
17 F.-M. Xu, J.-P. Xu, L.-P. Lv and J. Ji, *Soft Matter*, 2011, **7**, 1114–1120.
18 I. C. Riegel, A. Eisenberg, C. L. Petzhold and D. Samios, *Langmuir*, 2002, **18**, 3358–3363.
19 X. Liu, J.-S. Kim, J. Wu and A. Eisenberg, *Macromolecules*, 2005, **38**, 6749–6751.
20 A. Ebner, L. Wildling, A. S. M. Kamruzzahan, C. Rankl, J. Wruss, C. D. Hahn, M. Hölzl, R. Zhu, F. Kienberger, D. Blaas, P. Hinterdorfer and H. J. Gruber, *Bioconjugate Chem.*, 2007, **18**, 1176–1184.
21 R. C. Werlen, M. Lankinen, R. E. Offord, P. August Schubiger, A. Smith and K. Rose, *Cancer Res.*, 1996, **56**, 809–815.
22 T. Zhou, Z. D. Liu, H. Neubert, X. L. Kong, Y. M. Ma and R. C. Hider, *Bioorg. Med. Chem. Lett.*, 2005, **15**, 5007–5011.
23 I. Merino, J. D. Thompson, C. B. Millard, J. J. Schmidt and Y.-P. Pang, *Bioorg. Med. Chem.*, 2006, **14**, 3583–3591.
24 S. Kim, E. Kim, D.-S. Shin, H. Kang and K.-B. Oh, *Bioorg. Med. Chem. Lett.*, 2002, **12**, 895–898.
25 J. M. Hooker, A. Datta, M. Botta, K. N. Raymond and M. B. Francis, *Nano Lett.*, 2007, **7**, 2207–2210.
26 L. Zhang and J. P. Tam, *Anal. Biochem.*, 1996, **233**, 87–93.
27 P. E. Dawson and S. B. H. Kent, *Annu. Rev. Biochem.*, 2000, **69**, 923–960.
28 J. A. Borgia and G. B. Fields, *Trends Biotechnol.*, 2000, **18**, 243–251.
29 Y. Sohma and S. B. H. Kent, *J. Am. Chem. Soc.*, 2009, **131**, 16313–16318.
30 Y. Jin, L. Song, Y. Su, L. Zhu, Y. Pang, F. Qiu, G. Tong, D. Yan, B. Zhu and X. Zhu, *Biomacromolecules*, 2011, **12**, 3460–3468.
31 J. Chen, W. Zeng, R. Offord and K. Rose, *Bioconjugate Chem.*, 2003, **14**, 614–618.
32 C. J. Hawker, R. Lee and J. M. J. Frechet, *J. Am. Chem. Soc.*, 1991, **113**, 4583–4588.
33 M. Herrera, G. Manuschek and A. Kettrup, *J. Therm. Anal. Calorim.*, 2000, **59**, 385–394.
34 L. Song, C. Tu, Y. Shi, F. Qiu, L. He, Y. Jiang, Q. Zhu, B. Zhu, D. Yan and X. Zhu, *Macromol. Rapid Commun.*, 2010, **31**, 443–448.
35 M. Herrera, G. Matuschek and A. Kettrup, *Chemosphere*, 2001, **42**, 601–607.
36 J. Wang, M. Kuang, H. Duan, D. Chen and M. Jiang, *Eur. Phys. J. E: Soft Matter Biol. Phys.*, 2004, **15**, 211–215.
37 W. Cai, G.-T. Wang, Y.-X. Xu, X.-K. Jiang and Z.-T. Li, *J. Am. Chem. Soc.*, 2008, **130**, 6936–6937.
38 Y. Zhou and D. Yan, *Angew. Chem., Int. Ed.*, 2004, **43**, 4896–4899.
39 M. Yang, W. Wang, F. Yuan, X. Zhang, J. Li, F. Liang, B. He, B. Minch and G. Wegner, *J. Am. Chem. Soc.*, 2005, **127**, 15107–15111.
40 J.-X. Yang, X.-T. Tao, C. X. Yuan, Y. X. Yan, L. Wang, Z. Liu, Y. Ren and M. H. Jiang, *J. Am. Chem. Soc.*, 2005, **127**, 3278–3279.
41 C. B. Minkenberg, L. Florusse, R. Eelkema, G. J. M. Koper and J. H. van Esch, *J. Am. Chem. Soc.*, 2009, **131**, 11274–11275.
42 P. T. Corbett, J. Leclaire, L. Vial, K. R. West, J.-L. Wietor, J. K. M. Sanders and S. Otto, *Chem. Rev.*, 2006, **106**, 3652–3711.
43 J.-M. Lehn, *Science*, 2002, **295**, 2400–2403.